Rotational-Echo Double Resonance Characterization of Vancomycin Binding Sites in *Staphylococcus aureus*†

Sung Joon Kim,‡ Lynette Cegelski,§ Daniel R. Studelska,§ Robert D. O'Connor,§ Anil K. Mehta,§ and Jacob Schaefer*,§

Department of Molecular Biophysics, Washington University School of Medicine, and Department of Chemistry, Washington University, St. Louis, Missouri 63130

Received December 10, 2001

ABSTRACT: Solid-state NMR experiments with stable isotope-labeled *Staphylococcus aureus* have provided insight into the structure of the peptidoglycan binding site of a potent fluorobiphenyl derivative of chloroeremomycin (Eli Lilly LY329332). Rotational-echo double resonance (REDOR) NMR provided internuclear distances from the ^{19}F of this glycopeptide antibiotic to natural-abundance ^{31}P and to specific ^{13}C and ^{15}N labels biosynthetically incorporated into the bacteria from labeled alanine, glycine, or lysine in the growth medium. Results from experiments with intact late log phase bacteria and cell walls indicated homogeneous drug−peptidoglycan binding. Drug dimers were not detected in situ, and the hydrophobic fluorobiphenyl group of LY329332 did not insert into the bilayer membrane. A model of the binding site consistent with the REDOR results positions the vancomycin cleft around an un-cross-linked D-Ala-D-Ala peptide stem with the fluorobiphenyl moiety of the antibiotic near the base of a second, proximate stem in a locally ordered peptidoglycan matrix.

Vancomycin is reserved for the treatment of serious Gram-positive bacterial infection (*1*). Although vancomycin was introduced in the United States in the 1960s, its clinical use greatly increased in the 1980s because it was one of a few antimicrobial agents capable of killing methicillin-resistant staphylococci, including strains of *Staphylococcus aureus* (*2*−*5*). Vancomycin and other closely related glycopeptide agents (i.e., teicoplanin and avoparcin) inhibit the biosynthesis of the peptidoglycan of the bacterial cell wall (*6*). (The organization and chemical structure of the peptidoglycan of *S. aureus* are shown in Figure 1.) The antibiotics form complexes with the D-Ala-D-Ala carboxyl termini of the peptidoglycan precursor, presumably *N*-acetylglucosamine-*N*-acetylmuramyl-pentapeptide-pyrophosphorylundecaprenol (lipid II)[1] (*7*−*11*). Binding of vancomycin to lipid II could interfere with transglycosylase activity (*12*−*14*) and possibly transpeptidase activity as well (*15*), both of which are essential for the synthesis of new cell wall. The former extends the glycan chain and the latter cross-links the peptide stems with subsequent elimination of the terminal D-Ala. Cell wall and septa thinning ensue (*16*) because the balance between new cell wall synthesis at the cell membrane surface and enzymatic degradation of outer layers that normally functions to accommodate cell growth and division is dramatically perturbed.

Clinical isolates of glycopeptide-resistant enterococci were first characterized in Europe in 1986 (*17*, *18*). Resistant strains spread because they can colonize the lower gastrointestinal tract in the presence of most antibiotics. They are now a global problem and are a major source of hospital-based infections in the United States. Because of the ability of resistant strains to survive on surfaces outside their host environment, they readily infect patients undergoing antimicrobial therapy (*19*).

The basis of enterococci glycopeptide resistance, which is induced by exposure to glycopeptides, is the substitution of D-lactate or D-serine for D-alanine as the terminal residue of the carboxyl terminus of the peptidoglycan precursor. Several vancomycin-resistant phenotypes (e.g., VanA, VanB, VanC) have been characterized (*20*), and additional genotypes (e.g., *vanD*, *vanE*) have been recognized (*21*, *22*). Most contain a cluster of three genes essential for glycopeptide resistance. These genes encode enzymes that respectively catalyze the production of D-lactate (D-Lac) from pyruvate, preferentially ligate D-Lac to D-Ala, and preferentially hydrolyze D-Ala-D-Ala (*22*). The D-Ala-D-Ala to D-Ala-D-Lac alteration reduces the potency of vancomycin 1000-fold (*23*). In contrast, most laboratory (*24*) and clinically isolated (*22*) glycopeptide-resistant strains of *S. aureus* have thickened cell walls, some with enhanced antibiotic binding in the outer cell wall layers. However, the potential for transfer of a *van* gene cluster to *S. aureus* is a real and present danger.

† This work was supported by NIH Grant GM51554.

* To whom correspondence should be addressed. Phone: 314-935-6844. Fax: 314-935-4481. E-mail: schaefer@wuchem.wustl.edu.

‡ Department of Molecular Biophysics, Washington University School of Medicine.

§ Department of Chemistry, Washington University.

[1] Abbreviations: ΔS, $S_0 - S$, where S and S_0 are rotational-echo double resonance signal intensities with and without dephasing pulses, respectively; EDTA, ethylenediaminetetraacetic acid; HEPES, *N*-(2-hydroxyethyl)piperazine-*N*′-2-ethanesulfonic acid; f_{ct}, the number of alanyl [^{13}C]carbonyl carbons that are dipolar coupled to each fluorine of LY329332; lipid II, *N*-acetylglucosamine-*N*-acetylmuramyl-pentapeptide-pyrophosphorylundecaprenol; LY329332, 4-fluorobiphenyl derivative of chloroeremomycin; REDOR, rotational-echo double resonance; RMSD, root-mean-square deviation; SASM, *Staphylococcus aureus* synthetic medium; TPPM, two-pulse phase modulation; T_r, magic angle spinning rotor period; Tris, tris(hydroxymethyl)aminomethane.

10.1021/bi0121407 CCC: $22.00
Published on Web 05/09/2002

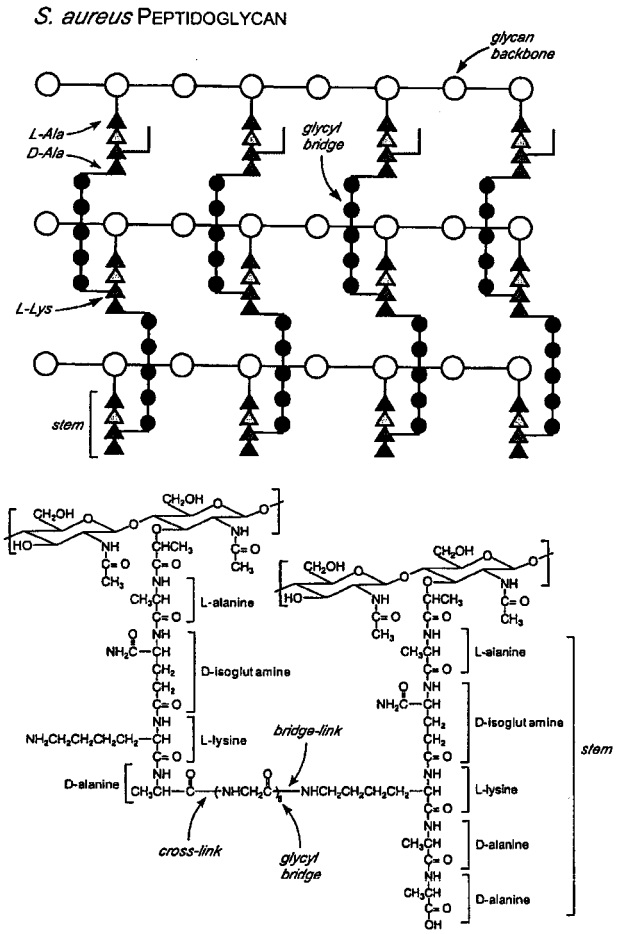

FIGURE 1: (Top) Schematic representation of an idealized version of the cell wall peptidoglycan of *S. aureus* (after Stryer). A four unit peptide stem (triangles) having the sequence L-Ala-D-Glu-L-Lys-D-Ala is attached to every second sugar of the glycan backbone (open circles). Cross-linking between glycans occurs through pentaglycyl bridges (dark circles) connecting the carbonyl carbon of D-Ala of the fourth position of one stem with the ϵ-nitrogen of L-Lys of the third position of another. (Bottom) Chemical structure of the peptidoglycan of *S. aureus*, with three sites identified for potential labeling: cross-link, bridge link, and pentaglycyl bridge. The five residue stem on the right has no cross-link to its D-Ala.

Solution-state NMR (*25*−*28*) supports the biochemical evidence (*7*−*11*, *29*) that vancomycin forms complexes with the D-Ala-D-Ala terminus of a peptidoglycan stem. The NMR studies were of drug complexes with model peptides and showed that binding of vancomycin to D-Ala-D-Ala involves the formation of five hydrogen bonds. This hydrogen bond network is perturbed by the replacement of the pentapeptide terminal D-alanine by D-lactate, which eliminates one H-bond and reduces vancomycin binding affinity (*30*).

Vancomycin derivatives with improved potency against both enterococci and staphylococci often have a hydrophobic chain of variable length attached to the vancomycin disaccharide amide nitrogen (Figure 2). Although these derivatives may have only a modestly increased affinity for model peptides in solution, their greatly increased potency implies highly specific binding in situ. This specificity is possibly enhanced by intermolecular interactions between the antibiotic (dimer formation) and between the antibiotic and the cell−lipid bilayer (membrane anchoring). The combination presumably leads to an overall reduced molecular mobility in the site of cell wall assembly and has been called the

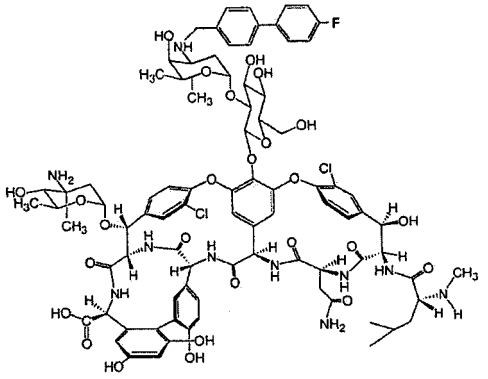

FIGURE 2: Chemical structure of a derviative of chloroeremomycin (Eli Lilly and Co. compound no. LY329332). This derivative differs from vancomycin by attachment of 4-epivancosamine to the sixth amino acid position of the vancomycin backbone and by the attachment of a 4-fluorobiphenyl moiety to the 4-epivancosamine of the fourth amino acid position.

"Gulliver effect" (*25*, *31*) because the vancomycin derivative is immobilized just as Gulliver was by the Lilliputians: by a *combination* of many, weak tie lines. However, vancomycin derivatives in which the aglycon D-Ala-D-Ala binding moiety has been altered or removed still retain some activity in vivo. This result has led to the suggestion (*32*) that some glycopeptide antibiotics may also target enzymes necessary for cell wall synthesis as well as the immediate cell wall precursors.

Rotational-echo double resonance (REDOR) has proven to be highly versatile in providing structural insights with atomic resolution for complicated heterogeneous solids such as amyloid plaques (*33*), membrane protein helical bundles (*34*, *35*), insect cuticle (*36*), and spider silk (*37*) that cannot be analyzed by X-ray diffraction or solution-state NMR. REDOR has also been used previously for the compositional and structural analysis of the ^{13}C- and ^{15}N-labeled peptidoglycan of *S. aureus* (*38*). In this paper we report the results of REDOR solid-state NMR experiments with the 4-fluorobiphenyl derivative of chloroeremomycin, a vancomycin analogue similar to the widely studied Lilly LY333328, except that fluorine replaces chlorine (*39*). The experiments were designed to characterize the in situ structure of the antibiotic binding site in stable isotope labeled mature peptidoglycan of cell walls and whole cells of *S. aureus.*

EXPERIMENTAL PROCEDURES

Vancomycin Derivative. LY329332 (Figure 2) is a chemical derivative of the naturally occurring glycopeptide chloroeremomycin, which is obtained synthetically by alkylating (with 4-fluorophenylbenzaldehyde) the 4-epivancosamine attached to the phenolic hydroxyl group of the fourth amino acid backbone position. Chloroeremomycin itself differs from vancomycin by the presence of 4-epivancosamine at the sixth amino acid backbone position. LY329332 is 1000-fold more potent than vancomycin in standard tests against vancomycin-resistant enterococci (*40*).

Growth and Labeling of Cell Walls and Whole Cells. S. aureus (ATCC 6538P) cells were grown in a defined medium (SASM), essentially as described by Tong et al. (*38*). SASM contained the following on a per liter basis: 10 g of D-glucose; 1 g each of $K_2HPO_4 \cdot 3H_2O$, KH_2PO_4, and $(NH_4)_2SO_4$; 0.2 g of $MgSO_4 \cdot 7H_2O$; 10 mg each of $MnSO_4 \cdot H_2O$,

$FeSO_4 \cdot H_2O$, and NaCl; 5 mg each of adenine, cytosine, guanine, uracil, and xanthine; 2 mg each of calcium pantothenate, thiamin hydrochloride, and niacin; 1 mg each of pyridoxine hydrochloride, riboflavin, inositol, $CuSO_4 \cdot 5H_2O$, and $ZnSO_4 \cdot 7H_2O$; 0.1 mg each of biotin and folic acid; and 0.1 g of all 20 common amino acids. The pH was adjusted to 7.0, and the medium was filter-sterilized by passage through a 0.2 μm membrane filter. To prepare samples for NMR spectroscopy, bacteria were grown in SASM in which the natural-abundance amino acids were replaced by L-[ϵ-^{15}N]lysine, [1-^{13}C]glycine, or D-[1-^{13}C]-alanine, either singly or in pairs. The cell wall sites that were targeted for labeling are shown in Figure 1 (bottom). A 5−8 mL SASM starter culture was grown overnight from a single colony at 37 °C at 250 rpm in a Environ-Shaker (Lab-Lines Instruments, Inc., Melrose Park, IL). Two milliliter aliquots of this were used to inoculate 300 mL of sterile SASM in 1 L flasks, which were grown under the same conditions to mid log phase, an absorbance of 1.0 at 660 nm. Intact cell NMR preparations were made from a single 300 mL growth; cell walls were typically prepared from parallel growth in three flasks. Bacteria were harvested by centrifugation at 10000*g* for 10 min at 4 °C in a Sorvall GS-3 rotor and washed once by resuspension in 300 mL of ice-cold 25 mM potassium phosphate buffer, pH 7.0 (cell walls), or twice in 300 mL of ice-cold 5 mM HEPES−NaOH or 40 mM triethanolamine hydrochloride, pH 7.0 (intact cells). Washed cells were pelleted and used for preparation of peptidoglycan cell walls or were resuspended in cold buffer for preparation of an intact cell NMR sample.

Peptidoglycan Cell Wall Isolation. Washed cells from 900 mL of mid log phase growth were resuspended in 50 mL of cold, sterile 0.025 M potassium phosphate, pH 7.0, containing 5 mg of DNase I (type II; Sigma-Aldrich, St. Louis, MO) and transferred to the 60 mL chamber of a Bead-Beater (Biospec Products, Bartlesville, OK), which was one-third full of 0.5 mm diameter glass beads. Cell disruption at 0 °C employed ten 1 min cycles separated by 1 min cooling periods. Glass beads were removed from the broken cells with a coarse sintered glass funnel and washed with 100 mL of 10 mM NaEDTA. The filtrate was centrifuged at 4 °C in a Beckman Ti 50.2 rotor at 25000*g* for 30 min. The crude cell wall pellet was resuspended in 10−20 mL of ultrafiltered nuclease-free grade I water (Solution 2000 water purifier, model 2002BL; Aqua Solution, Inc., Jasper, GA) and added dropwise with stirring to 100 mL of boiling 4% sodium dodecyl sulfate. After being boiled for 30 min, the suspension was allowed to cool for 2 h with stirring, after which it was allowed to stand unstirred overnight at room temperature. It was then sedimented by centrifugation at 60000*g* for 20 min at room temperature and washed three times with water. The pellet was resuspended in 60 mL of 0.01 M Tris buffer, pH 8.2, containing 16 mg each of trypsin (type I; Sigma-Aldrich, St. Louis, MO) and chymotrypsin (type II; Sigma-Aldrich, St. Louis, MO) and 5 mg of DNase I. The suspension was incubated at 37 °C with stirring for 16 h and then sedimented at 100000*g* for 1 h at 20 °C and washed three times with water. The yield was typically 55 mg of isolated cell walls.

Lyophilization of Cell Walls and Intact Cells Complexed with LY329332. Each NMR sample contained 2.0 μmol (3.6 mg) of LY329332 in a complex with isolated cell walls or intact cells. Cell walls (20 or 40 mg) were diluted in 9.75 mL of ice-cold 5 mM HEPES, pH 7.0, in an 80 mL lyophilization flask to which LY329332 was added for a 5 min incubation on ice. To this was added concentrated trehalose, to produce a suspension of drug-complexed cell walls in 18 mM trehalose and 5 mM HEPES, pH 7.0, at a final volume of 10 mL. The flask was placed in a regulated low-temperature bath (endocal ULT 80; Neslab Instruments Inc., Newington, NH) set to −6 °C. After equilibration at −6 °C, the bath was set to −40 °C. The suspension froze at approximately −14 °C. After 2 h at −40 °C, the flask was cooled in liquid nitrogen and attached to a lyophilizer. After a vacuum of 5 mTorr was achieved, the liquid nitrogen was removed to begin lyophilization. Intact cells from a 300 mL mid log phase growth were initially complexed with LY329332 in a fashion similar to that of cell walls, in 18 mM trehalose and 5 mM HEPES, pH 7.0, at a final volume of 10 mL. This excipient mix was abandoned in favor of 40 mM triethanolamine hydrochloride, pH 7.0, at a final volume of 12 mL. Triethanolamine buffer produced a superior cake after lyophilization that supported the weight of the bacteria without collapse. We believe that this desirable effect is due to hydrogen bond interactions of buffer hydroxyl groups with the bacteria because triethylamine hydrochloride was not effective at the same concentration. It is possible that triethanolamine hydrochloride, a volatile buffer (*41*), may be a better water replacement reagent for some lyophilized samples than disaccharides such as trehalose (*42*).

Binding Assay. One microliter of a 15 mg/mL isolated cell wall suspension was added to 250 μL of solutions containing vancomycin (or LY329332) of varying concentration. After being mixed and vortexed, the resulting cell wall complex was centrifuged at 2500*g* for 15 min at 4 °C. The concentration of antibiotic in the supernatant was determined by optical density measurements at 280, 290, 295, and 305 nm, calibrated by solutions of known concentration.

REDOR NMR. Solid-state NMR was performed using a six-frequency transmission line probe (*43*) having a 12 mm long, 6 mm inside diameter analytical coil and a Chemagnetics/Varian ceramic spinning module. Lyophilized cell wall and whole cell samples were contained in thin wall Chemagnetics/Varian 5 mm outside diameter zirconia rotors. The rotors were typically spun at 6250 or 7463 Hz with the speed under active control to within ±2 Hz. The spectrometer was controlled by a Tecmag pulse programmer. Radio-frequency pulses for ^{31}P (202 MHz), ^{13}C (125 MHz), and ^{15}N (50.7 MHz) were produced by 1 and 2 kW American Microwave Technology power amplifiers. ^{1}H (500 MHz) and ^{19}F (470 MHz) radio-frequency pulses were generated by 1 kW Creative Electronics tube amplifiers driven by 50 W American Microwave Technology power amplifiers. The π pulse lengths were 8 μs for ^{31}P, 10 μs for ^{13}C and ^{15}N, and 5 μs for ^{19}F.

REDOR was used to restore the dipolar coupling between heteronuclear pairs of spins that is removed by magic angle spinning (*44*). REDOR experiments are always done in two parts, once with rotor synchronized dephasing pulses (S) and once without (S_0). The dephasing pulses change the sign of the heteronuclear dipolar coupling, and this interferes with the spatial averaging resulting from the motion of the rotor. The difference in signal intensity ($\Delta S = S_0 - S$) for the observed spin in the two parts of the REDOR experiment is directly related to the corresponding distance to the dephasing

spin (*45*). REDOR dephasing is generally plotted as S/S_0 or $\Delta S/S_0$ so that homogeneous decay (T_2) of the observed magnetization is removed. Typical REDOR pulse sequences are found in the literature both in simple (*45*) and refined forms (*33*−*36*). The accuracy of distance measurements using ^{19}F dephasing pulses was confirmed using the two-bond coupling of [^{19}F]polycarbonate as described previously (*46*). Standard XY-8 phase cycling (*47*) was used for all dephasing pulses. A 12 T static magnetic field was provided by an 89 mm bore Magnex superconducting solenoid. Proton−carbon cross-polarization transfers were made in 2 ms at 50 kHz. Proton dipolar decoupling was 100 kHz during data acquisition; TPPM of the ^{1}H radio frequency (*48*) was used throughout both dipolar evolution and decoupling periods.

Calculated REDOR Dephasing. Dephasing was calculated using the Bessel function expressions given by Mueller et al. (*49*) and de la Caillerie and Fretigny (*50*) for a spin $^1/_2$ pair. For the [1-^{13}C]alanine cell wall data, this expression was summed over a Gaussian distribution of dipolar couplings corresponding to a distribution of isolated ^{13}C−^{19}F pairs. The distribution parameters (mean and width) and overall scaling were allowed to vary to minimize the root-mean-square deviation (RMSD) between the experimental and calculated dephasing (*51*). Because only a fraction of peptidoglycan binding sites were occupied, scaling (determined by the results of the binding assay) was necessary to account for ^{13}C labels that are not near a ^{19}F label. These ^{13}C labels contributed only to the full echo but not the REDOR difference. For the dephasing calculation of the bridge labeled by [1-^{13}C]glycine, a five glycyl α helix was assembled and energy minimized using Insight II (MSI, San Diego, CA). The grid position of a single ^{19}F label relative to the pentaglycyl helix was varied, and the RMSD was minimized between the experimental and calculated dephasing. A 20% weighting was assumed for the contribution to dephasing from each of the five carbonyl carbons of the helix.

Modeling. A model of the complex of the fluorobiphenyl chloroeremomycin derivative LY329332 was generated using Insight II and Swiss PDB Viewer (Glaxo Wellcome Research). The conformation of the cleft of the vancomycin analogue (binding pocket) was modeled using hydrogen bond restraints from solution-state NMR results of vancomycin bound to the L-Lys-D-Ala-D-Ala tripeptide (*31*). This model was manually docked into the peptidoglycan structure without energy minimization. POV-Ray (team-coord@povray.org) was used to create the illustration of the cell wall complex. Spacings between glycan chains were taken from low- and medium-angle X-ray diffraction of bacterial peptidoglycan (*52*). Stem and bridge lengths were estimated from previous REDOR experiments (*36*).

RESULTS

Binding Assay. A nonlinear least-squares fit to an independent, identical binding site model (Figure 3) yielded K_D = 3.6 μM (vancomycin) and 4.5 μM (LY329332), with B_{max} (as total number of binding sites per milligram of isolated cell wall) = 0.45 μmol (vancomycin) and 0.35 μmol (LY329332). The binding of vancomycin was slightly more complicated for whole cell suspensions. No attempt was made at a quantitative determination of binding constants for whole cells, although qualitatively cell wall and whole cell binding was similar. Estimates of binding site occupancy in whole cells were made by comparison to that of cell walls.

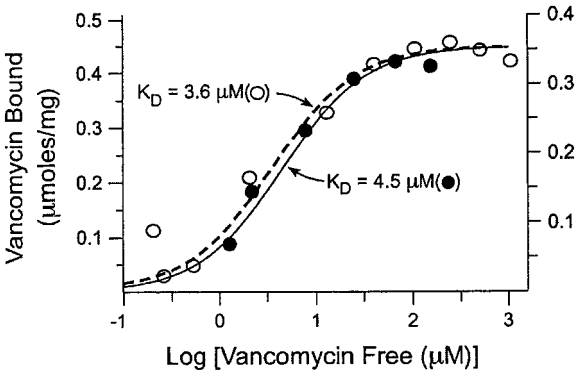

FIGURE 3: Binding of vancomycin (open circles, left-hand scale) and LY329332 (closed circles, right-hand scale) to isolated cell walls of *S. aureus*. These data show that the enhanced potency of LY329332 (which is 1000-fold greater than that of vancomycin against vancomycin-resistant enterococci) is not related to an increase in binding affinity for mature peptidoglycan. The dissociation constant for vancomycin is in reasonable agreement with values for binding of vancomycin to L-Lys-D-Ala-D-Ala tripeptide model compounds.

REDOR NMR. The ^{13}C{^{19}F} REDOR full-echo NMR spectrum (Figure 4, bottom left) of LY329332 complexed with cell walls isolated from *S. aureus* (16% binding site occupancy) grown on media containing [1-^{13}C]glycine is dominated by the carbonyl carbon peak at 171 ppm (Figure 1). This peak arises from labeled carbons in the pentaglycyl bridge and has a chemical shift consistent with an α-helical conformation for the bridge (*53*). (All cytoplasmic proteins and amino acids have been removed from the sample.) Isotopic ^{13}C enrichment of glycine for this sample is estimated at 65% (*38*). The peak near 70 ppm is due to the sugar carbons of the excipient trehalose. Natural-abundance [^{13}C]peptidoglycan peaks appear between 20 and 60 ppm. Their weak intensities are consistent with no significant natural-abundance background contribution to the major 170 ppm peak.

Only the pentaglycyl ^{13}C label is associated with a significant REDOR difference signal (Figure 4, top left). The relative intensities of the REDOR differences for the spinning sidebands after 8 T_r are different from those of the corresponding full echoes, a comparison which is particularly noticeable for spinning at 3125 Hz (Figure 4, right). After just eight rotor cycles of dipolar evolution, only the glycyl carbonyl carbon closest to the fluorine (with the strongest ^{13}C−^{19}F dipolar coupling) contributes to the REDOR difference signal. Differences in dephasing rates for the sidebands of this label indicate a preference in the orientation of the ^{13}C−^{19}F vector relative to the [^{13}C]carbonyl carbon chemical shift tensor (*51*).

The ^{13}C{^{19}F} dephasing ($\Delta S/S_0$) for the sum of centerband and sidebands of the pentaglycyl bridge increases by more than a factor of 4 for a change of dipolar evolution time from 5 to 20 ms (Figure 5). This dephasing is consistent with that expected from multiple dipolar couplings. (Details of the calculated dephasing shown in Figure 5 by the solid line are in the Discussion.)

Cell walls isolated from *S. aureus* grown in the presence of D-[1-^{13}C]alanine have incorporation of label in L-Ala at

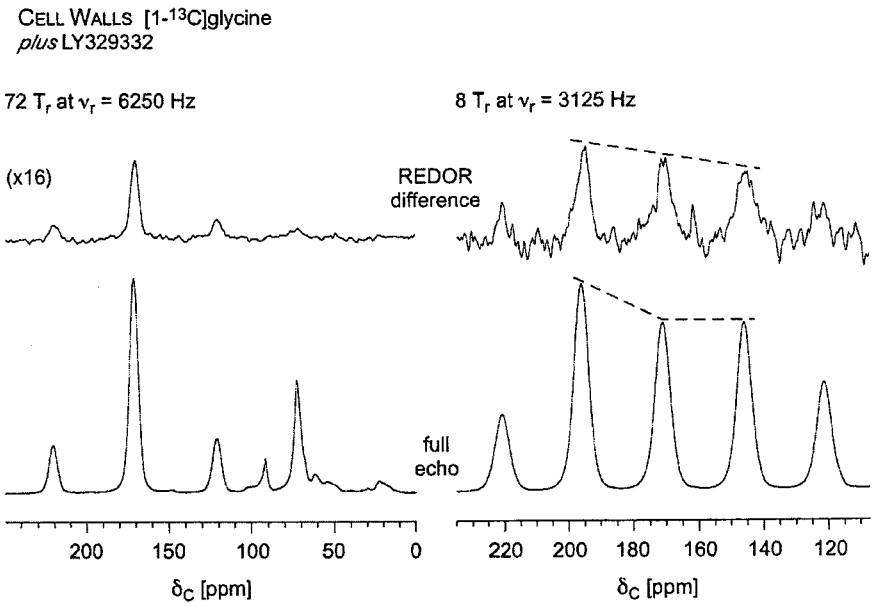

FIGURE 4: $^{13}C\{^{19}F\}$ REDOR NMR spectra for a complex of LY329332 with the cell walls of *S. aureus* grown on media containing [1-^{13}C]-glycine. REDOR differences (ΔS) are shown at the top of the figure and the full echoes (S_0) at the bottom. $\Delta S = S_0 - S$, where S and S_0 are the signal intensities with and without ^{19}F dephasing pulses, respectively. Expanded frequency scale plots of the carbonyl carbon regions of the REDOR spectra after eight rotor cycles of dipolar evolution (only the signal of the labeled carbonyl carbon nearest to ^{19}F is dephased) are shown to the right of the figure. The dissimilarity of the REDOR difference and full-echo spectra (dotted lines) indicates an orientational preference for the $^{13}C-^{19}F$ internuclear vector relative to the [^{13}C]carbonyl carbon chemical shift tensor (*51*).

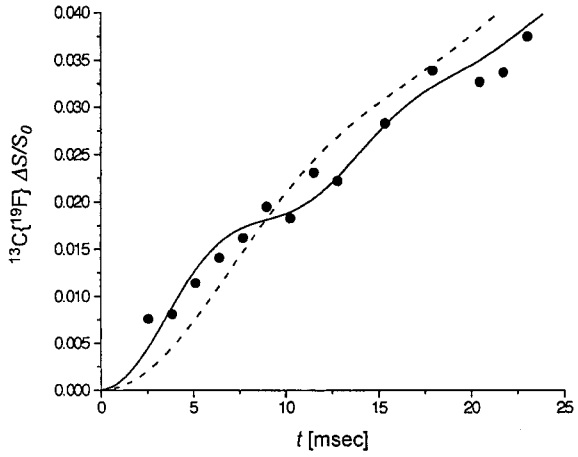

FIGURE 5: $^{13}C\{^{19}F\}$ REDOR dephasing ($\Delta S/S_0$) as a function of the dipolar evolution time, t, for a complex of LY329332 with the cell walls (circles) of *S. aureus* grown on media containing [1-^{13}C]-glycine. The binding site occupancy for 2 μmol of the antibiotic complexed to the cell walls was 16%. The solid line shows the calculated dephasing assuming the $^{13}C-^{19}F$ distances of the model shown in Figure 9. The breaks in the calculated dephasing arise from the presence of five significantly different $^{13}C-^{19}F$ dipolar couplings. The dotted line shows the calculated dephasing if the ^{19}F label is assumed not to be near one end or the other of the bridge as shown in Figure 9 but rather is assumed to be near the middle of the bridge.

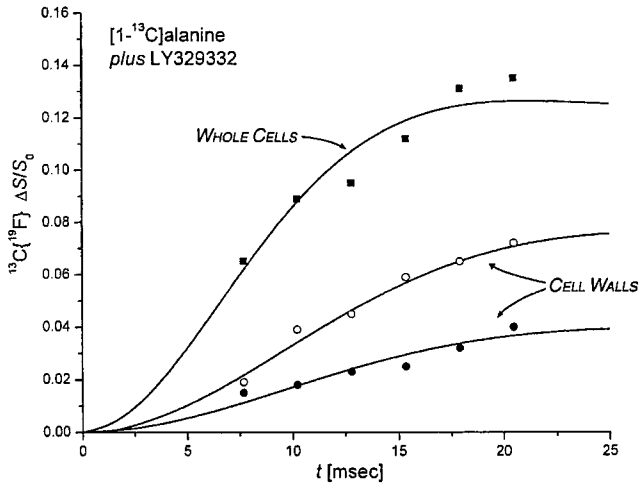

FIGURE 6: $^{13}C\{^{19}F\}$ REDOR dephasing ($\Delta S/S_0$) as a function of the dipolar evolution time, t, for complexes of LY329332 with whole cells (squares) and cell walls (circles) of *S. aureus* grown on media containing D-[1-^{13}C]alanine. The binding site occupancy of LY329332 complexed to whole cells was 33% (solid squares) and complexed to cell walls either 33% (open circles) or 16% (closed circles). The full-echo S_0 of the cell wall sample was used in plotting the whole cell dephasing, consistent with the same count of occupied binding sites indicated by the binding assay of Figure 3 for 2 μmol of LY329332 bound to either 20 mg of cell walls or 140 mg of whole cells (dry weights). The calculated cell wall dephasing (solid lines) assumed a Gaussian distribution of distances for isolated $^{13}C-^{19}F$ pairs centered at 7.6 Å with a width of 1.5 Å. The calculated whole cell dephasing used the same distribution but was centered at 6.8 Å.

the base of the pentapeptide stem, as well as in the D-Ala-D-Ala terminus of the stem. The $^{13}C\{^{19}F\}$ REDOR dephasing for these cell wall samples with 16% or 33% of vancomycin binding sites occupied (Figure 6, circles) is reasonably well described (Figure 6, solid lines) by a narrow Gaussian distribution of $^{13}C-^{19}F$ dipolar couplings, centered at 7.6 Å with a full width at half-height of 1.5 Å. The total dephasing for cell wall samples (Figure 6, circles) shows that the fraction of carbons contributing to S_0 that are also coupled to fluorine is 8% (for 33% occupancy) and 4% (for 16% occupancy). The absolute $^{13}C\{^{19}F\}$ REDOR dephasing (ΔS) for whole cells labeled by D-[1-^{13}C]alanine complexed to LY329332 (Figure 6, solid squares) is about double that observed for the corresponding cell wall complex. The full-echo S_0 of the cell wall sample was used in plotting the whole cell dephasing. This scaling seems reasonable because the

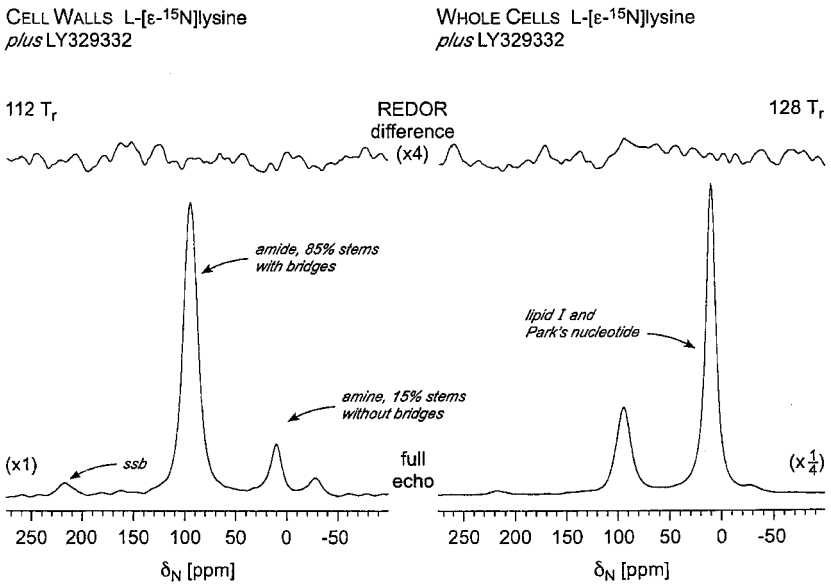

FIGURE 7: $^{15}N\{^{19}F\}$ REDOR NMR spectra for complexes of LY329332 with cell walls (left) and whole cells (right) of *S. aureus* grown on media containing L-[ϵ-^{15}N]lysine. The binding site occupancy for 2 μmol of the antibiotic complexed to both cell walls and whole cells was 33%. The REDOR differences (ΔS) after 112 (left) and 128 (right) rotor cycles of dipolar evolution are shown at the top of the figure and the corresponding full echoes (S_0) at the bottom. The absence of a detectable difference signal indicates that the $^{15}N-^{19}F$ internuclear separation in both cell wall and whole cell complexes (binding site occupancy of 33%) is greater than 9 Å. Each spectrum was the result of the accumulation of approximately 100K scans. The magic angle spinning was at 6250 Hz.

binding assay of Figure 3 showed equal numbers of occupied binding sites for 2 μmol of LY329332 bound to either 20 mg of cell walls or 140 mg of whole cells (dry weights). On the basis of the binding site assay, the cell walls therefore represented approximately 15% of the dry weight of the whole cells. Somewhat stronger $^{13}C-^{19}F$ dipolar coupling was found for the whole cell dephasing relative to that for cell walls. The same Gaussian distribution of couplings was used for the whole cell dephasing but was centered at 6.8 Å rather than 7.6 Å. The calculated dephasing plateau for the whole cell complex is 13% (Figure 6).

The ^{15}N full-echo spectrum of cell walls isolated from *S. aureus* grown on media containing L-[ϵ-^{15}N]lysine has a major amide nitrogen peak and a minor amine nitrogen peak (Figure 7, bottom left). The amide peak is due to lysines in stems with pentaglycyl bridges attached and the amine peak to lysines in stems with no bridge attached (Figure 1, bottom). The relative intensities of the two peaks are about 7:1. The full-echo spectrum from similarly labeled whole cells shows an amide peak approximately equal in intensity to that of the cell wall spectrum (Figure 7, bottom right). This result means that the natural-abundance ^{15}N contribution to the amide peak from cytoplasmic proteins is minor. The amine nitrogen peak in whole cells is significantly greater than that in cell walls (Figure 7, bottom). Because the lysine label does not scramble (*38*), we infer that the amine nitrogen peak arises from the high concentration of peptidoglycan precursors in whole cells that do not yet have pentaglycyl bridges attached, the so-called lipid I and Park's nucleotide (*12*, *13*, *54*−*55*). The whole cell, full-echo ^{15}N NMR spectrum was scaled assuming that 15% of the dry weight of the whole cells is due to cell walls (see previous paragraph). Neither the cell wall nor the whole cell sample has a significant $^{15}N\{^{19}F\}$ REDOR difference (Figure 7, top) even though both samples contained LY329332 at 33% occupancy.

The $^{31}P\{^{19}F\}$ REDOR difference for the cell wall complex is also negligible (Figure 8, left). The only source of phosphorus in this sample is teichoic acid, a polyphosphate that represents about 30% of the *S. aureus* cell wall by weight (*56*). The whole cell complex has a full-echo signal intensity about three times that of the cell wall complex (Figure 8, bottom right). Most of this increase in intensity is due to cytoplasmic phosphates; the concentration of phosphorus of the headgroups of the membrane bilayer of the whole cells is only about one-tenth the concentration of the main-chain phosphates of teichoic acid (*57*). The whole cell complex shows a broad 1% REDOR difference signal (Figure 8, top right). The centers of the cell wall and whole cell ^{31}P full-echo peaks are shifted from one another by about 400 Hz (2 ppm), presumably the result of the different chemical environments of the various types of ^{31}P in the whole cells.

DISCUSSION

Potency and Binding Affinity. The dissociation constant for vancomycin is 3.6 μM (Figure 3), in reasonable agreement with values for binding of vancomycin to L-Lys-D-Ala-D-Ala tripeptide model compounds, as determined by capillary electrophoresis (*58*), surface plasmon resonance (*59*), and electron spray ionization mass spectrometry (*60*). The dissociation constant for LY329332 (4.5 μM, Figure 3) is close to that reported (*39*) for the chlorinated analogue, LY333328. These data show that the enhanced potency of LY329332 and that of the chlorinated analogue (both 1000-fold greater than that of vancomycin against vancomycin-resistant enterococci) are not reflected in an increase in binding affinity for mature peptidoglycan.

LY329332 Proximity to Stem Alanines. On the basis of compositional analysis (*56*), a 20 mg lyophilized cell wall sample and a 140 mg lyophilized whole cell sample both have about 12 μmol of peptidoglycan peptide stems. The assay of Figure 3 was used to establish that 2.0 μmol of

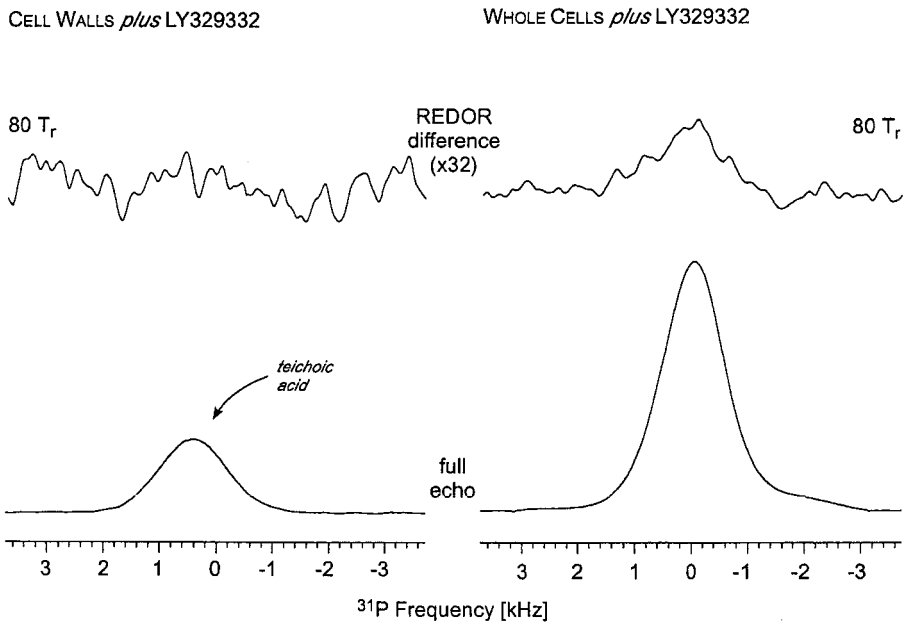

FIGURE 8: ^{31}P{^{19}F} REDOR NMR spectra for complexes of LY329332 with cell walls (left) and whole cells (right) of *S. aureus*. These are the same complexes whose ^{15}N REDOR spectra are shown in Figure 6. The REDOR differences (ΔS) after 80 rotor cycles of dipolar evolution are shown at the top of the figure and the full echoes (S_0) at the bottom. The absence of a detectable difference signal for the cell wall sample indicates that the average ^{31}P−^{19}F internuclear separation between the phosphorus of teichoic acid and the fluorine of the vancomycin derivative is greater than 18 Å. The spectra on the left were the result of the accumulation of 100K scans, and those on the right of 250K scans, with a data acquisition period that was commensurate with the rotor period. The spectra are the result of Fourier transforms of rotor-echo maxima and represent the quantitative sums of the centerbands and all spinning sidebands. The magic angle spinning was at 7462 Hz (the displayed spectral width).

complexed LY329332 (3.6 mg) corresponds to 33% binding site occupancy. This means that half of the stems of the cell wall and whole cell samples of the peptidoglycans of the samples of Figures 4−8 are binding sites (2/12 divided by 0.33 is 1/2). Assuming, to a first approximation, that LY329332 must complex to stems ending in D-Ala-D-Ala, half of the stems end in D-Ala-D-Ala and half in D-Ala. The large number of stems ending in D-Ala-D-Ala is consistent with the low activity of D,D-carboxypeptidase in *S. aureus* (*61*, *62*). Thus, each peptidoglycan peptide stem has, on average, 1.0 L-Ala and 1.5 D-Ala for a total of 2.5 alanyls per stem. The alanyl side groups of the teichoic acid component of the cell walls were removed under the high pH of the isolation procedure (*63*) so that the total number of stem alanyl carbonyl carbons contributing to the cell wall REDOR S_0 of Figure 6 is just 2.5. This number, as well as the cell wall S_0, was used to analyze the whole cell dephasing, which is described in the next paragraph. Use of the cell wall S_0 to scale the whole cell $\Delta S/S_0$ avoids counting contributions from whole cell teichoic acid and cytoplasmic proteins, which are irrelevant to peptidoglycan binding.

An active alanine racemase in *S. aureus* ensures that both L-Ala and D-Ala of peptidoglycan stems are equivalently labeled regardless of which ^{13}C-labeled isomer was provided in the growth medium. De novo synthesis of alanine results in an isotopic ^{13}C dilution to 40−50% for both L-Ala and D-Ala of the peptide stems (*38*) although, for a REDOR analysis, the exact isotopic enrichment is not important. The 13% value of the dephasing plateau for the whole cell complex with 33% of the vancomycin binding sites occupied (Figure 6) can be used to calculate the number of alanyl carbonyl carbons (f_{cf}) that are coupled to each vancomycin fluorine as $(1/2)(1/3)(f_{cf}/2.5) = 0.13$. The first factor on the left is the fraction of stems that bind, the second factor is the binding site occupancy, and the third factor is the fraction of stem alanyl carbonyl carbons that are coupled to a fluorine. Thus, $f_{cf} = 2$; that is, each vancomycin fluorine is coupled to just two alanyl carbonyl carbons.

LY329332 Proximity to the Pentaglycyl Bridge. On the basis of the ^{13}C{^{19}F} REDOR experiments on cell wall complexes (Figure 5), the ^{19}F of LY329332 is near a pentaglycyl bridge connecting two stems. About 50% of stems are not binding sites and so presumably end in D-Ala. Another 15% of all stems have no bridges attached (see the lysylamine nitrogen peak, Figure 7, bottom left) and so necessarily result in adjacent stems ending in D-Ala-D-Ala. If all stems that are not binding sites are assumed to end in D-Ala-D-Ala, then an additional 35% of stems must have a bridge attached but no cross-link connection to an adjacent stem. This assumption seems extreme. It requires that about one-third of all attached bridges are open, that is, not part of cross-links. Direct measures (*38*,) of the concentration of open bridges in mature peptidoglycan place this number at no more than 10−15%. In addition, REDOR determinations of the concentration of D-[1-^{13}C]Ala-D-[^{15}N]Ala in the peptidoglycan stems of *S. aureus* suggest that less than 50% of all stems end in D-Ala-D-Ala (*18*). Thus, it is possible that substantially more than 50% of all stems end in D-Ala but that some of these stems may be binding sites in whole cell peptidoglycan. This situation would decrease the requirement for open bridges. Regardless of the situation for full binding site occupancy, we feel that it is safe to assume that for low levels of bound LY329332, which is the situation for all of our experiments, all occupied binding sites are stems ending in D-Ala-D-Ala.

The distribution of peptidoglycan structures that we will assume is summarized as follows: At 16% binding site occupancy, there is one vancomycin for each 12 stems. The

number of pentaglycyl bridges per bound vancomycin therefore is (0.85)(12) = 10. The 85% factor is the experimentally determined fraction of stems with no bridges attached (Figure 7, left). If there are 10 bridges for each complexed LY329332, then the expected dephasing plateau for the carbonyl carbons of the pentaglycyl bridge in intact peptidoglycan of whole cells is approximately 10%. The bridges are far enough apart that is unlikely for two bridges to be near any single LY329332 (cf. below). However, assuming the same sort of decrease in total dephasing for the bridge carbonyls of an isolated cell wall sample relative to a whole cell sample that was observed for the stems in Figure 6, this plateau would be reduced to about 6%. (The justification for this reduction in the dephasing plateau is discussed in more detail in the following paragraph.) The total observed dephasing shown in Figure 5 is consistent with the assumptions above about cell wall composition. The dephasing, which has not reached a plateau after 22 ms, is about 4%. This value also indicates that most of the glycyl carbonyl carbons of a bridge near a bound vancomycin are within dephasing range of the ^{19}F.

We attribute the decreased ^{13}C{^{19}F} REDOR dephasing plateau of the cell wall complex compared to that of the whole cells (Figure 6) to a partial disruption of nearest neighbor proximities of stems. The isolation of the cell walls creates fragments that are likely to have reduced possibilities for ^{13}C−^{19}F coupling. Indeed, the absence of contact with the ^{31}P of teichoic acid for the cell wall complex (Figure 8, left) is indicative of partial disruption of the peptidoglycan long-range order. Paradoxically, the disruption of the peptidoglycan structure in whole cells to create isolated cell walls leads to more homogeneous vancomycin binding (Figure 3). Presumably, only those peptidoglycan sites that are locked into position by multiple covalent cross-links retain their shape during the cell wall isolation procedure. Thus, the LY329332 binding sites in the cell wall sample represent a subset of the whole cell binding sites, which leads to more homogeneous binding.

Figure 9 shows the allowed positions of the ^{19}F relative to the five carbonyl carbons of a compact α-helical bridge (*38*), consistent with the REDOR dephasing of Figures 4 and 5. These positions were used to calculate the dephasing shown in Figure 5 (solid line). The fluorine can be near one end of the bridge or the other but not near the middle (Figure 5, dotted line). This orientational preference is consistent with that obtained from the differences in the sideband dephasing rates (Figure 9, black dots). The spread of possible positions for the fluorine label is an indication of the uniqueness of the model given the available signal-to-noise ratios and the associated experimental scatter and uncertainty shown in Figure 5. The nearest glycyl carbonyl carbon is 5 Å from the ^{19}F and the most distant is 11 Å, both values accurate to 20%. The calculated dephasing plateau is 6%. The absence of an ^{15}N{^{19}F} REDOR difference for the amide nitrogen connecting the bridge to the stem (Figure 7, left) rules out placement of the fluorine at that end of the bridge (the bridge link end). The fluorine must therefore be positioned near the cross-link site of the bridge.

D-*Ala and* L-*Ala.* If the fluorine is near a bridge cross-link, it is necessarily also close to the single D-Ala carbonyl carbon of the cross-link. To satisfy the $f_{cf} = 2$ condition, the second alanyl carbonyl carbon must therefore be the single

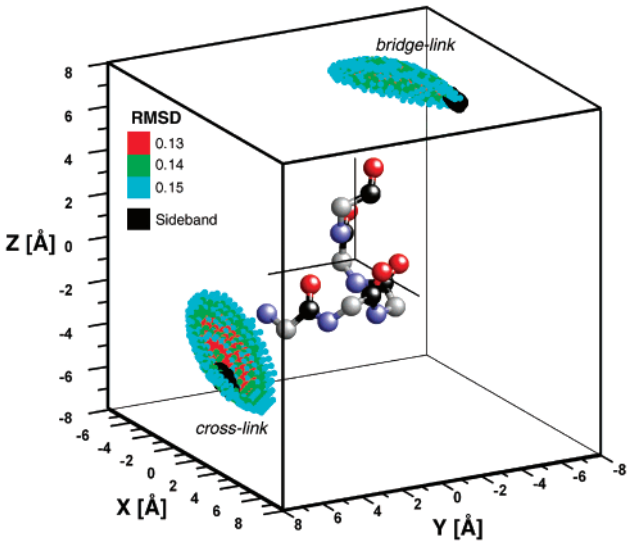

FIGURE 9: Possible positions for the ^{19}F of LY329332 (small dots) relative to the pentaglycyl helix (carbonyl carbons in black, C_α in gray, nitrogens in blue, and oxygens in red) consistent with the REDOR dephasing of Figures 5 and 6. The colors of the ^{19}F positions indicate the RMSD between calculated and experimental dephasing. The best match shown (red) has a 13% error and the worst match (blue) a 15% error. Most likely placements of ^{19}F relative to the end carbonyl carbons determined by analysis of the spinning sideband intensities of Figure 5 (right) are shown in black. The bridge link site is near the top cluster and the cross-link site near the bottom cluster. The absence of a ^{15}N{^{19}F} REDOR difference for the amide nitrogen connecting the bridge to the stem (see Figure 10, left) rules out placement of the ^{19}F near the bridge link.

L-Ala at the base of a peptide stem. If the fluorine were near the tip of an un-cross-linked stem, f_{cf} would be 3, which is not consistent with the whole cell dephasing plateau of Figure 6. For the D-Ala and L-Ala carbonyl carbons both to be 7.6 Å from the ^{19}F, they must be on the same stem. Typical distances from carbonyl carbons on neighboring stems are more than 10 Å (cf. below). Note that this discussion is based on carbonyl carbons not ^{13}C labels. There are very few stems having multiple ^{13}C labels because of the relatively low isotopic enrichment.

Model of the Binding Site. A model illustrating these relationships is shown in Figure 10. The model assumes that the vancomycin cleft binds to a stem terminating in D-Ala-D-Ala. This sort of termination is indicated by a ball at the end of the stem. The cross-link is attached offset from the idealized stem cylinder (for example, see the cross-link at center, left, of Figure 10). The peptidoglycan of *S. aureus* has about 10−20 layers of glycans (*64*), only two of which are shown in Figure 10. The center-to-center separation of glycan planes is 40 Å (*52*). In addition, the glycan chains in both layers are shown for clarity as strictly parallel, which need not be the case; chains in adjacent layers may be oblique or rotated about their long axes relative to one another. In the model, the fluorine of the biphenyl moiety is not near the L-Ala of the complexed stem, but rather the L-Ala of a nearest neighbor stem on an adjacent glycan strand. This nearest neighbor stem is shown with a bridge (85% of all stems have bridges), and this arrangement is the source of ^{19}F coupling to the carbonyl carbons of D-Ala and Gly. The complex is presumably stabilized by interactions of the sugars of LY329332 with proximate glycans. One of these possible

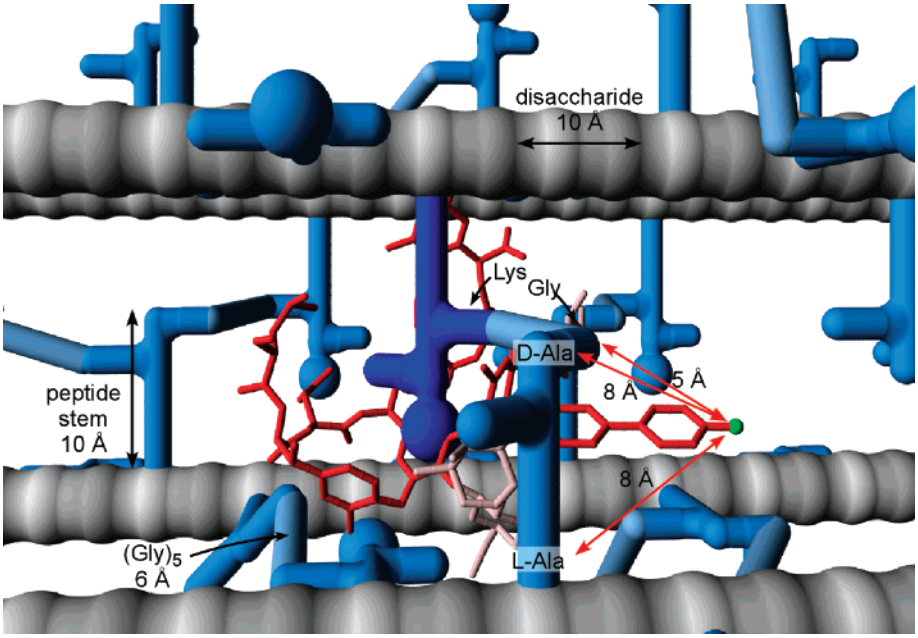

FIGURE 10: Model of the binding of LY329332 in the mature peptidoglycan of *S. aureus*. The glycan strands are shown as gray cylinders, the peptide stems as blue cylinders, and the pentaglycyl bridges as light blue cylinders. The helical pitch of the glycan chain places adjacent stems on the same chain at right angles to one another. Stems ending in D-Ala-D-Ala have a ball at the end. The vancomycin cleft is shown attached to a stem (dark blue) ending in D-Ala-D-Ala. The sugar side chains of LY329332 are shown in white, and the ^{19}F label is in green. The ^{19}F is 8 Å from the carbonyl carbon of the L-Ala at the base of the peptide stem in the center foreground, 8 Å from the carbonyl carbon of D-Ala at the tip of this stem, and 5 Å from the carbonyl carbon of Gly_5 of the pentaglycyl bridge cross-linked to this stem. Other experimentally established distances are in black.

interactions is shown in the center foreground; the other is obscured by the cross-link of the complexed stem in the foreground. The model of Figure 10 is meant to be suggestive and should not be considered a final structure. LY329332 has been manually docked to a D-Ala-D-Ala terminus of a peptide stem, and the resulting peptidoglycan model of the complex has not been energy minimized. More experimental REDOR restraints are needed to refine the model, particularly restraints to remove some of the ambiguities of ^{19}F placement near the pentaglycyl bridge.

Binding Site Homogeneity. The narrowness of the Gaussian distributions of distances used to describe the $^{13}C\{^{19}F\}$ REDOR dephasing for cell walls and whole cells labeled by [^{13}C]alanine (Figure 6) suggests a strong similarity between binding sites. The distance and preferred orientational restraints to the nearby [^{13}C]glycine-labeled bridges are similarly tight although some variability can be tolerated (Figure 9). We conclude that LY329332 binding to mature peptidoglycan is uniform and reasonably homogeneous, at least in the 0−33% occupancy range.

Membrane Anchors and Drug Dimers. The potency of vancomycin derivatives is commonly ascribed to their hydrophobic tails (for example, the fluorobiphenyl moiety of LY329332) acting as a membrane anchor (*31*), which then preferentially situates the antibiotic to disrupt peptidoglycan synthesis. The anchor is thought to be further stabilized by drug dimerization (*65*−*67*). Back-to-back dimers are stabilized by sugar−sugar interactions and face-to-face dimers by an array of hydrogen bonds and hydrophobic interactions (*68*). Neither a drug anchor nor a drug dimer has been used in building the model of Figure 10. If the fluorobiphenyl tail of LY329332 were indeed buried in the cell membrane, then the $^{31}P\{^{19}F\}$ REDOR difference of Figure 8 (left) would represent an F−P internuclear distance of at least 8 Å. This estimate of the minimum distance assumes that all of the LY329332 is at the interface, that all of the dephasing is due to headgroup ^{31}P, that each headgroup phosphorus of the outer lipid layer is coupled to one fluorine, and that the full-echo ^{31}P signal intensity from half of the bilayer headgroups is 5% of the teichoic acid, cell wall, full-echo signal (*57*). This estimate is inconsistent with the observed ^{19}F dipolar couplings to ^{13}C labels in alanyl and glycyl stem and bridge carbonyl carbons. If the fluorobiphenyl tail were 8 Å below the bilayer headgroup, the ^{19}F would simply be too far from the nearest stem to show any measurable dipolar coupling. We therefore conclude that the fluorobiphenyl moiety of LY329332 is not a preferential membrane anchor, at least in the mature peptidoglycan samples of Figures 6 and 7. We ascribe the minor whole cell $^{31}P\{^{19}F\}$ $\Delta S/S_0$ of Figure 8 (right) to incidental ^{19}F contact with structural (as opposed to cell surface) teichoic acid ^{31}P.

A restraint on the formation of LY329332 dimers in mature cell walls is that they must be consistent with the observed $^{13}C\{^{19}F\}$ $\Delta S/S_0$ of Figures 4−6. This means that the ^{19}F must be proximate to a bridge and two nearest neighbor stems, as shown in Figure 10. Because most bridges are closed at both ends in mature peptidoglycan (i.e., both a cross-link and a bridge link are in place), only one of the nearest neighbor stems connected by a bridge can have a D-Ala-D-Ala terminus and therefore be a binding site with a defined orientational preference. In our modeling, we have not been able to satisfy the experimental homogeneous REDOR restraints using dimers. We conclude that LY329332 does not form dimers in situ in mature peptidoglycan and that the many possible sugar interactions with the glycans of the cell walls provide ample stabilization of a monomeric complex. However, this conclusion may not be true for the binding of LY329332 with immature cell walls and lipid II.

At the membrane−peptidoglycan interface, two proximate stems need not be cross-linked, the bridge can be open, and a face-to-face dimer could form.

Vancomycin Mode of Action. The model of Figure 10 describing LY329332 binding to mature cell walls provides several restraints for the most prevalent binding site available for glycopeptide antibiotics in *S. aureus*. However, the structure of this site provides no direct information about the killing action of LY329332. In fact, some bacteria simply thicken their peptidoglycan to protect against vancomycin and its analogues (*22*−*24*). Insights into the mode of action of vancomycins can be gained by the sort of REDOR analysis illustrated here for mature cell walls, performed instead on drug complexes with cell wall precursors formed *during* growth in actively dividing cells. This work is in progress.

SUMMARY

The 4-fluorobiphenyl derivative of chloroeremomycin (LY329332, a vancomycin analogue from Eli Lilly Co.) binds homogeneously as a monomer to a peptide stem of the mature peptidoglycan of whole cells of *S. aureus*. When 16% of the cell wall binding sites are occupied, there are 12 peptide stems and 10 pentaglycyl bridges per bound drug molecule. The hydrophobic tail of LY329332 is not part of a membrane anchor but rather is near a second peptide stem and the cross-link site of its attached pentaglycyl bridge. These proximities are established unambiguously by measuring through-space dipolar couplings between ^{13}C and ^{15}N labels incorporated into the cell walls and the fluorine of the vancomycin analogue using rotational-echo double resonance (REDOR) magic angle spinning NMR. Binding sites of the peptidoglycans of cell wall extracts are similar to those of whole cells, but with the second stem and attached bridge sometimes missing. This occurs in the isolated cell walls presumably because of disruption in the cell wall chain packing. The disruption is seen in the diminution of the REDOR dephasing plateau (maximum total dephasing) with little decrease in the average $^{13}C-^{19}F$ dipolar coupling. The model of the binding site consistent with all available REDOR distance restraints is, at this point, more than a cartoon and has some testable predictive capabilities but is not yet a full molecular structure.

ACKNOWLEDGMENT

The authors thank Dr. Richard C. Thompson and Dr. Thalia I. Nicas (Lilly Research Laboratories, Indianapolis, IN) for drug potency test results prior to publication and for a generous supply of LY329332.

REFERENCES

1. Reynolds, P. E. (1989) *Eur. J. Clin. Microbiol. Infect. Dis. 8*, 943−950.
2. Sieradzki, K., and Tomasz, A. (1996) *FEMS Microbiol. Lett. 142*, 161−166.
3. Kirby, W. M. (1981) *Rev. Infect. Dis. 3* (Suppl.), S236−239.
4. Harvey, K., and Pavillard, R. (1982) *Med. J. Aust. 1*, 465−467.
5. Sapico, F. L., Montgomerie, J. Z., Canawati, H. N., and Aeilts, G. (1981) *Am. J. Med. Sci. 281*, 101−109.
6. Reynolds, P. E., and Somner, E. A. (1990) *Drugs Exp. Clin. Res. 16*, 385−389.
7. Perkins, H. R. (1969) *Biochem. J. 111*, 195−205.
8. Nieto, M., and Perkins, H. R. (1971) *Biochem. J. 123*, 773−787.
9. Perkins, H. R. (1982) *Pharmacol. Ther. 16*, 181−197.
10. Barna, J. C., and Williams, D. H. (1984) *Annu. Rev. Microbiol. 38*, 339−357.
11. Perkins, H. R., and Nieto, M. (1974) *Ann. N.Y. Acad. Sci. 235*, 348−363.
12. Matsuhashi, M., Dietrich, C. P., and Strominger, J. L. (1965) *Proc. Natl. Acad. Sci. U.S.A. 54*, 587−594.
13. Anderson, J. S., Matsuhashi, M., Haskin, M. A., and Strominger, J. L. (1967) *J. Biol. Chem. 242*, 3180−3190.
14. Brotz, H., Bierbaum, G., Reynolds, P. E., and Sahl, H. G. (1997) *Eur. J. Biochem. 246*, 193−199.
15. Reynolds, P. E., and Somner, E. A. (1990) *Drugs Exp. Clin. Res. 16*, 385−389.
16. Molitor, E., Kluczny, C., Brotz, H., Bierbaum, G., Jack, R., and Sahl, H. G. (1996) *Zentralbl. Bakteriol. 284*, 318−328.
17. Leclercq, R., Derlot, E., Duval, J., and Courvalin, P. (1988) *N. Engl. J. Med. 319*, 157−161.
18. Uttley, A. H., Collins, C. H., Naidoo, J., and George, R. C. (1988) *Lancet i*, 57−58.
19. Martone, W. J. (1998) *Infect. Control Hosp. Epidemiol. 19*, 539−545.
20. Arthur, M., Reynolds, P., and Courvalin, P. (1996) *Trends Microbiol. 4*, 401−407.
21. Perichon, B., Reynolds, P., and Courvalin, P. (1997) *Antimicrob. Agents Chemother. 41*, 2016−2018.
22. Fraimow, H. S., and Courvalin, P. (2000) Resistance to glycopeptides in gram-positive pathogens, in *Gram-Positive Pathogens* (Fischetti, V. A., Novick, R. P., Ferretti, J. J., Portnoy, D. A., and Rood, J. I., Eds.) pp 621−634, ASM Press, Washington, DC.
23. Liu, J., Volk, K. J., Lee, M. S., Pucci, M., and Handwerger, S. (1994) *Anal. Chem. 66*, 2412−2416.
24. Sieradzki, K., and Tomasz, A. (1997) *J. Bacteriol. 179*, 2557−2566.
25. Williams, D. H. (1996) *Nat. Prod. Rep.*, 469−477.
26. Kalman, J. R., and Williams, D. H. (1980) *J. Am. Chem. Soc. 102*, 897−905.
27. Williams, H., and Butcher, D. W. (1981) *J. Am. Chem. Soc. 103*, 5700−5704.
28. Williams, D. H., and Kalman, J. (1977) *J. Am. Chem. Soc. 99*, 2768−2774.
29. Wright, G. D., and Walsh, C. T. (1992) *Acc. Chem. Res. 25*, 468−473.
30. Walsh, C. T., Fisher, S. L., Park, L.-S., Prahalad, M., and Wu, Z. (1996) *Chem. Biol. 3*, 21−28.
31. Beauregard, D. A., Williams, D. H., Gwynn, M. N., and Knowles, D. J. C. (1995) *Antimicrob. Agents Chemother. 39*, 781−785.
32. Ge, M., Chem, Z., Onishi, H. R., Kohler, J., Silver, L. L., Kerns, R., Fukuzawa, S., Thompson, C., and Kahne, D. (1999) *Science 284*, 507−511.
33. Balbach, J. J., Ishii, Y., Antzutkin, O. N., Leapman, R. D., Rizzo, N. W., Dyda, F., Reed, J., and Tycko, R. (2000) *Biochemistry 39*, 13748−13759.
34. Smith, S. O., Kawakami, T., Liu, W., Ziliox, M., and Aimoto, S. (2001) *J. Mol. Biol. 313*, 1139−1148.
35. Wang, J., Balazs, Y. S., and Thompson, L. K. (1997) *Biochemistry 36*, 1699−1703.
36. Merritt, M. E., Christensen, A. M., Kramer, K. J., Hopkins, T. L., and Schaefer, J. (1996) *J. Am. Chem. Soc. 118*, 11278−11282.
37. Michal, C. A., and Jelinski, L. W. (1998) *J. Biol. NMR 12*, 231−241.
38. Tong, G., Pan, Y., Dong, H., Pryor, R., Wilson, G. E., and Schaefer J. (1997) *Biochemistry 36*, 9859−9866.
39. Allen, N. E., LeTourneau, D. L., and Hobbs, J. N., Jr. (1997) *J. Antibiot. 50*, 677−684.
40. Allen, N. E., LeTourneau, D. L., and Hobbs, J. N., Jr. (1997) *Antimicrob. Agents Chemother. 41*, 66−71.
41. Stoll, V. S., and Blanchard, J. S. (1990) *Methods Enzymol. 182*, 24−49.

42. Prestrelski, S. J., Arakawa, T., and Carpenter, J. F. (1993) *Arch. Biochem. Biophys. 303*, 465.
43. Schaefer, J., and McKay, R. A. (1999) U.S. Patent 5,861,748.
44. Gullion, T., and Schaefer, J. (1989) *J. Magn. Reson. 81*, 196−200.
45. Gullion, T., and Schaefer, J. (1989) *Adv. Magn. Reson. 13*, 58−83.
46. Goetz, J. M., Wu, J. H., Yee, A. F., and Schaefer, J. (1998) *Solid State NMR 12*, 87−95.
47. Gullion, T., Baker, D. B., and Conradi, M. S. (1990) *J. Magn. Reson. 89*, 479−484.
48. Bennett, A. E., Rienstra, C. M., Auger, M., Lakshmi, K. V., and Griffin, R. G. (1995) *J. Chem. Phys. 103*, 6951−6958.
49. Mueller, K. T., Jarvie, T. P., Aurentz, D. J., and Roberts, B. W. (1995) *Chem. Phys. Lett. 242*, 535−542.
50. de la Caillerie, J.-B. d'E., and Fretigny, C. (1998) *J. Magn. Reson. 133*, 273−280.
51. O'Connor, R. D., and Schaefer, J. (2002) *J. Magn. Reson. 154*, 46−52.
52. Labischinski, H., Barnickel, G., Brakaczek, H., and Giesbrecht, P. (1979) *Eur. J. Biochem. 95*, 147−155.
53. Saitô, H. (1986) *Magn. Reson. Chem. 24*, 835−852.
54. Reynolds, P. (1961) *Biochim. Biophys. Acta 52*, 403.
55. Anderson, J. S., Meadow, P. M., Haskin, M. A., and Strominger, J. L. (1966) *Arch. Biochem. Biophys. 116*, 487−515.
56. Dobson, B. C., and Archibald, A. R. (1978) *Arch. Microbiol. 119*, 295−301.
57. Umeda, A., Yokoyama, S., Arizono, T., and Amako, K. (1992) *J. Electron Microsc. 41*, 46−52.
58. Rao, J., Colton, I. J., and Whitesides, G. M. (1997) *J. Am. Chem. Soc. 119*, 9336−9340.
59. Rao, J., Yan, L., Xu, B., and Whitesides, G. M. (1999) *J. Am. Chem. Soc. 121*, 2629−2630.
60. van de Kerk-van Hoof, A., and Heck, A. J. (1999) *J. Antimicrob. Chemother. 44*, 593−599.
61. Archibald, A. R., Baddiley, J., and Heptinstall, S. (1973) *Biochim. Biophys. Acta 291*, 629−634.
62. Tipper, D. J., and Strominger, J. L. (1965) *Proc. Natl. Acad. Sci. U.S.A. 54*, 1133−1141.
63. Tipper, D. J., and Strominger, J. L. (1968) *J. Biol. Chem. 267*, 11248−11254.
64. Gieswbrecht, Kersten, T., Maidhof, H., and Wecke, J. (1998) *Microbiol. Mol. Biol. Rev. 62*, 1371−1414.
65. Westwell, M. S., Bardsley, B., Dancer, R. J., Try, A. C., and Williams, D. H. (1996) *Chem. Commun.*, 580−590.
66. Schafer, M., Schneider, T. R., and Sheldrick, G. M. (1996) *Structure 4*, 1509−1515.
67. Loll, P. J., Miller, R., Weeks, C. M., and Axelsen, P. H. (1998) *Chem. Biol. 5*, 293−298.
68. Loll, P. J., and Axelsen, P. H. (2000) *Annu. Rev. Biophys. Biomol. Struct. 29*, 265−289.

BI0121407